The Astrophysical Journal, 741:74 (9pp), 2011 November 10 doi:10.1088/0004-637X/741/2/74

INFRARED SPECTROSCOPY OF GAS-PHASE POLYCYCLIC AROMATIC HYDROCARBON CATIONS IN THE 10–50 μm SPECTRAL RANGE

Joost M. Bakker[1], Britta Redlich[1], Alexander F. G. van der Meer[1,3], and Jos Oomens[1,2]
[1] FOM Institute for Plasma Physics Rijnhuizen, P.O. Box 1207, 3430 BE Nieuwegein, The Netherlands
[2] Van 't Hoff Institute for Molecular Sciences, University of Amsterdam, Science Park 904, 1098 XH Amsterdam, The Netherlands
[3] Institute for Molecules and Materials, Radboud University Nijmegen, Heyendaalseweg 135, 6525 AJ Nijmegen, The Netherlands
Received 2011 May 3; accepted 2011 August 3; published 2011 October 19

ABSTRACT

The gas-phase infrared spectra of four polycyclic aromatic hydrocarbon (PAH) cations have been recorded in the 10–50 μm (or 1000–200 cm^{-1}) spectral range via IR multiple photon dissociation (IRMPD) spectroscopy. Ionized PAHs are formed by UV laser ionization in an effusive beam and subsequently irradiated with a single pulse of narrowband tunable infrared light produced by the Free-Electron Laser for IntraCavity Experiments FELICE. The ion population is then analyzed in a time-of-flight mass spectrometer. Upon resonance, dissociation is induced so that IR spectra can be recorded by monitoring either the depleted parent ion intensity or the appearance of fragment ions as a function of the wavelength. The intracavity IR fluence enables the recording of IRMPD spectra of strongly bound PAH cations in the hitherto inaccessible far-IR spectral range. Experimental spectra are presented for the radical cations of anthracene, tetracene, pentacene, and coronene. Spectra calculated with density functional theory at the B3LYP/6-311g(2df,2pd) level reproduce IR frequencies reasonably accurately in this spectral range when a uniform scaling factor of 0.94 over the complete 10–50 μm spectral range is employed. We show that even vibrational modes with a calculated IR intensity lower than 1 km mol^{-1} can be observed. For the catacondensed PAH cations we find CH out-of-plane bending vibrations involving four adjacent CH groups within a few wavenumbers of 733 cm^{-1}, closely matching the 13.6 μm UIR band. For the larger systems, pentacene and coronene, we observe a continuous structureless background absorption above 400 cm^{-1} which is attributed to the high density of IR dipole allowed combination modes for these systems.

Key words: infrared: ISM – ISM: molecules – methods: laboratory – molecular data – molecular processes

Online-only material: color figures

1. INTRODUCTION

It has become widely accepted that there is an abundant presence of large carbonaceous molecules in interstellar environments. Although very few individual species have been identified, carbon chains, polycyclic aromatic hydrocarbons (PAHs), fullerenes, and diamond-like species have all been suggested to occur. Recently, the spectral fingerprints of fullerene C_{60} and C_{70} have been detected in the infrared (IR) emission spectrum of the planetary nebulae Tc1 (Cami et al. 2010) and several reflection nebulae (Sellgren et al. 2010). The IR emission features detected in the spectra recorded by the Infrared Spectrograph (Houck et al. 2004) on board the *Spitzer Space Telescope* (Werner 2004) showed an excellent match with laboratory spectra. The abundant presence of fullerenes is likely limited to hydrogen-poor environments, since the presence of substantial amounts of hydrogen inhibits fullerene formation while favoring that of PAHs (De Vries et al. 1993; Wang et al. 1995).

It is now generally accepted that PAHs, in particular in their cationic form, are responsible for the characteristic IR emission patterns from the interstellar medium (ISM) (Allamandola et al. 1985; Léger & Puget 1984; Tielens 2008). However, in contrast to the recent identification of fullerenes, no direct match for an individual PAH molecule has been established to date. This is perhaps not surprising since there are no known "magic numbers," i.e., a few highly stable PAHs (or "Grand-PAHs") toward which the formation is strongly biased, as in the case of fullerenes. Nevertheless, attempts to identify specific PAHs responsible for interstellar emission features have led to a high laboratory and theoretical activity aimed at providing accurate IR spectral data. With the extension of available observational data into the far-IR with *Spitzer*, and the future extension toward even longer wavelengths with *Herschel* (Pilbratt et al. 2010), the need for laboratory data at longer wavelengths has become urgent. This range may be of special interest for the identification of individual PAH species as the spectra are known to be species specific at long wavelengths, where especially vibrational modes involving deformations of the carbon framework are located (Boersma et al. 2011; Mattioda et al. 2009; Ricca et al. 2010).

Over the past two decades much effort has been devoted to the establishment of a catalog of PAH infrared spectra based on matrix-isolation (MI) spectroscopy (Bauschlicher et al. 2010; Hudgins & Allamandola 1995a, 1995b, 1997; Hudgins et al. 1994, 2000; Mattioda et al. 2003; Szczepanski et al. 1993, 1995a, 1995b; Szczepanski & Vala 1993). Recently, MI spectroscopy has been applied to study the spectra of neutral PAHs down to 100 cm^{-1} (Mattioda et al. 2009). Although it is known that MI data may deviate from gas-phase spectra (Joblin et al. 1994), various recent gas-phase spectra revealed band positions that are in very good agreement with those reported in MI studies (Oomens et al. 2000, 2001a, 2001b, 2003; Piest et al. 2001).

To record the mid- and far-IR absorption properties of strongly bound ions in the gas phase, IR multiple photon dissociation (IRMPD) spectroscopy has been developed (Oomens et al. 2000, 2006). In this technique, the sequential resonant absorption of many IR photons activates the ion. When the internal energy reaches the dissociation threshold, fragmentation ensues. The mass-spectrometric detection of fragment ions then signals IR absorption. While this technique has yielded a wealth of spectral information, its applicability at longer wavelengths

is limited by the increasing imbalance between the energy deposited per IR photon and the constant fragmentation energy. This imbalance can be mitigated by lowering the internal energy barrier, for instance by forming complexes of the species of interest with weakly bound messenger atoms or molecules. The dissociation energy threshold of such a complex is substantially lower than that for unimolecular decay of the uncomplexed species (typically 0.1 eV versus several eV), thus lowering the number of photons required to induce dissociation (Okumura et al. 1985; Piest et al. 1999, 2001; Ricks et al. 2009).

As an alternative to complexation, the efficiency of IR excitation can be enhanced. All IR action spectroscopy experiments on bare PAH cations have been carried out at IR Free-Electron Laser (IR-FEL) facilities, making use of the exceptional brightness of these laser sources. Recently, a new extension to the FELIX facility has been constructed where the gas-phase species can be exposed to the IR radiation inside the cavity of the FEL (Bakker et al. 2010). Under these conditions, the excitation efficiency is substantially enhanced, thus expanding the spectral range over which IRMPD spectroscopy can be successfully applied.

Here we present the IRMPD spectra for a series of PAH cations down to 200 cm^{-1}, corresponding to 50 μm. We recorded spectra for the catacondensed PAH cations anthracene ($C_{14}H_{10}^+$), tetracene ($C_{18}H_{12}^+$), and pentacene ($C_{22}H_{14}^+$), as well as for a pericondensed PAH cation, coronene ($C_{24}H_{12}^+$). Hudgins & Allamandola have previously reported MI based ion spectra for these species down to ~700 cm^{-1} (Hudgins & Allamandola 1995a). Kong and co-workers have addressed the low-wavenumber region for the tetracene and pentacene using $(1 + 1')$ zero electron kinetic energy (ZEKE) spectroscopy (Zhang et al. 2008, 2010). It is important to note, however, that selection rules in ZEKE schemes are different so that they do not give direct access to the IR spectra in the ground state of the ion.

2. EXPERIMENT

IRMPD spectra of PAH cations are obtained using the molecular beam instrument on the first beam line of the Free-Electron Laser for IntraCavity Experiments (FELICE) described previously (Bakker et al. 2010). In contrast to earlier studies on gas-phase cationic PAHs (Oomens et al. 2000), the ions are not confined in a radio-frequency ion trap. Instead, the experiments are carried out in an effusive beam formed by vaporization of the PAHs in an oven. While this approach does not allow for mass isolation prior to IR laser interaction, it has the benefit of mass analysis using a standard Wiley–McLaren-type time-of-flight (TOF) mass spectrometer. The mass resolution of this detection method allows one to resolve the loss of atomic hydrogen, which forms the lowest energy-loss channel (Ekern et al. 1998; Jochims et al. 1999).

An effusive beam of PAH molecules is created by subliming a sample of the solid PAH (Sigma Aldrich, used without further purification). The molecules are ionized by a counter-propagating laser pulse of an ArF excimer laser (193 nm, Neweks PSX-100, ~3 mJ) shaped by an aperture to approximately 1.5 mm in diameter). A few μs after preparation, the ions are crossed by the IR light produced by FELICE at right angles.

FELICE laser pulses are produced in a pulse train, the so-called macropulse, with a typical duration of approximately 5 μs, consisting of picosecond-long micropulses at 1 ns separation. The optical pulse at the interaction point consists of two pulse trains that are shifted between 0 and 0.5 ns with respect to each other depending on the (variable) distance between the interaction point and the end mirror of the laser cavity. The reader is referred to Bakker et al. (2010) for further details. The radiation is near transform limited and the spectral width can be adjusted between typically 0.4% and 2% FWHM of the central frequency. For the experiments described here, the typical bandwidths used are 0.5% FWHM with macropulse energies of about 2 J. A few μs after interacting with FELICE all ions are pulse extracted into a Wiley–McLaren linear TOF mass spectrometer with an approximately 650 mm long flight tube. Ions are detected on a 25 mm diameter microchannel plate detector. The transients are recorded by a 100 MHz, 400 MS s^{-1} digitizer (Acqiris DP310). To reduce long-term signal fluctuations, the experiment is run at twice the FELICE macropulse repetition rate (10 Hz); the transients produced in the absence of the IR beam are recorded as reference mass spectra.

Because of the high energy per macropulse, it is necessary to adjust the fluence with which the ions interact to avoid saturation of the IRMPD spectra. This is accomplished by adjusting the distance between the FELICE focus and the interaction region, which is achieved by translating the whole experimental apparatus along the FELICE laser beam. The distance to the focus can be changed between 0 and 300 mm; with a Rayleigh range of the FELICE laser beam of 55 mm this allows for a variation of a factor 30 in power density.

In the IRMPD process, an ion is heated by sequential absorption of multiple photons on-resonance with a vibrational transition. Each photon absorption is followed by rapid energy redistribution over all vibrational degrees of freedom of the ion. Interestingly, this process is the reverse of the adopted mechanism for IR emission of UV-excited species in the ISM (Barker et al. 1987; Cook & Saykally 1998). With increasing internal energies, vibrational anharmonicities induce a redshift in the absorbing or emitting vibrational mode, which leads to spectral broadening and redshifting in both mechanisms (Joblin et al. 1995; Oomens et al. 2006). Current quantum-chemical models fail to accurately calculate these anharmonicities at high internal energies necessary to model the IR emission spectra of PAHs. On the other hand, these anharmonicities are implicitly encoded into the IRMPD spectra in the magnitude of the redshift with respect to the fundamental transitions (Oomens et al. 2003).

Experimental IRMPD spectra are compared to theoretical linear absorption spectra generated by quantum-chemical calculations using the Gaussian03 program package (Frisch et al. 2004). The geometries of all PAH cations are optimized using the B3LYP functional with the 6-311g(2df,2pd) basis set and harmonic frequencies are calculated at the same level. To correct calculated harmonic frequencies for the inherent vibrational anharmonicity, a uniform scaling factor is commonly applied, amounting to about 0.98 for the level of theory employed here (Andersen & Uvdal 2005). The redshifts in IRMPD spectra described above require the use of a smaller scaling factor; in this work, an empirical scaling factor of 0.94 is used for all species, giving quantitative agreement over the entire spectral range investigated.

3. RESULTS AND DISCUSSION

Figure 1 depicts two typical mass spectra for the anthracene cation, which are representative for all PAH ions under study in this work. Trace (a) is a reference mass spectrum showing the mass distribution without FELICE irradiation. Trace (b) shows a mass spectrum with FELICE tuned to 732 cm^{-1}, with the interaction zone at a distance of around 300 mm from the laser

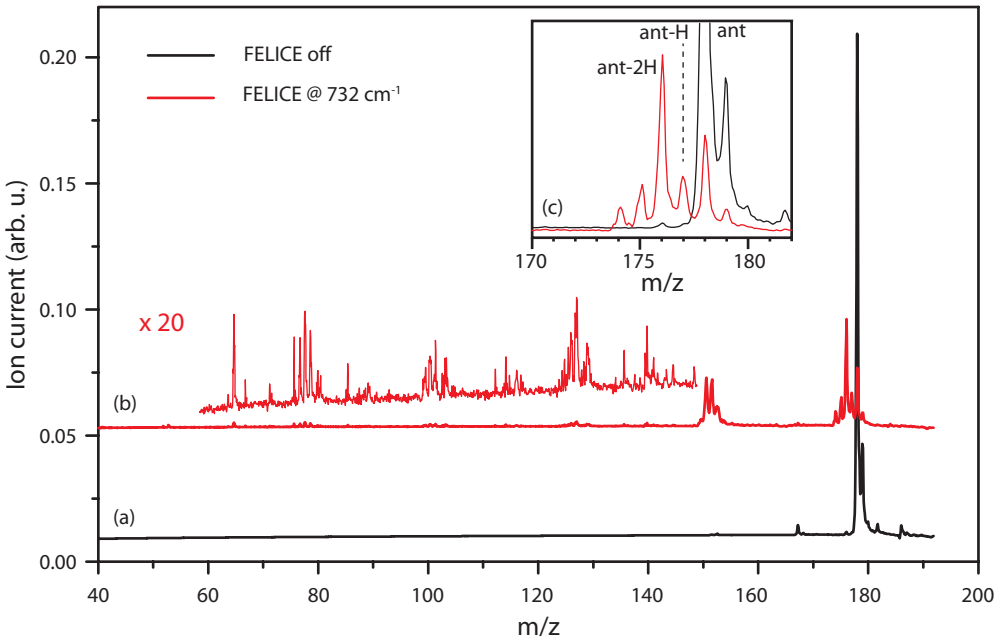

Figure 1. Mass spectra of anthracene recorded without FELICE (a) and with FELICE tuned to 732 cm^{-1} (b). The inset (c) shows a zoom of the two mass spectra around the parent ion mass.

(A color version of this figure is available in the online journal.)

focus. At this point the FELICE waist is 2.8 mm, which is larger than the approximately 1.5 mm diameter excimer laser beam. One observes a dramatically different mass spectrum with roughly 80% of the original anthracene signal depleted and a broad distribution of fragment ions. There is substantial loss of one and two hydrogen atoms (1H- and 2H-loss, respectively), as well as loss of C_2H_x groups. This observation is consistent with previously observed mass spectra of the anthracene cation after (V)UV photodissociation (Ekern et al. 1998; Jochims et al. 1999; Ling & Lifshitz 1998; Ling et al. 1997) or collisional activation with argon (Wang et al. 1997). In line with photoionization studies, but contrary to collisional activation, the relative abundance for 2H-loss is substantially higher than for 1H-loss, which is shown in the close-up in Figure 1. Directly above trace (b) a 20-fold zoom of the mass spectrum below $m/z = 140$ is shown where a wide variety of $C_{14-n}H_{10-m}^+$ fragment ions is visible.

Due to the large number of fragmentation channels, it is difficult to obtain a proper measure of the IR absorption cross section from the appearance of fragment ions. However, since the depletion is substantial and the IR laser beam is larger than the ion cloud we can transform the depletion of the parent ion channel into a relative IR absorption cross section by the formula $\sigma \propto -\ln(s_{\rm fel}/s_{\rm ref})$, where $s_{\rm fel}$ and $s_{\rm ref}$ are the ion intensities for the PAH cation of interest with and without FELICE radiation, respectively. For weak IR resonances, the only fragments observed are those associated with the loss of one or two H atoms. As can be seen in the inset in Figure 1, there is only a small population in the 2H-loss channel when FELICE is off, and it is well resolved from the parent ion peak. The relative IR absorption cross section is then obtained by $\sigma \propto s_{\rm 2H}/s_{\rm PAH}$, where $s_{\rm PAH}$ and $s_{\rm 2H}$ are the ion intensities for the PAH cation of interest and for the 2H-loss channel, respectively, provided $s_{\rm 2H} \ll s_{\rm PAH}$. For each ion we will therefore present a spectrum based on depletion and, in ranges with weak absorptions only, one based on the appearance of the fragments associated with 2H-loss.

3.1. Anthracene

The IRMPD spectrum of cationic anthracene obtained via depletion of the parent ion is depicted by the full black line in the top part of Figure 2. The spectrum is recorded with the interaction point at 300 mm from the FELICE focus. A total of four peaks are observed, at 421, 732, 882, and 944 cm^{-1}, respectively. Below the experimental spectrum a calculated stick spectrum is shown, where the harmonic frequencies are scaled by 0.94; the ordinate shows the calculated integrated intensities. To facilitate comparison with the IRMPD spectrum, the stick spectrum is also shown as convoluted with a Gaussian line shape (15 cm^{-1} Gaussian width, or ~35 cm^{-1} FWHM). The observed resonances together with their calculated frequencies and a description of the associated vibrational motions are collected in Table 1. Excellent agreement between the predicted linear IR spectrum and the experimentally observed IRMPD spectrum is observed. The four strong resonances are associated to CH out-of-plane (o.o.p.) vibrations, i.e., concerted motions of the hydrogens through the molecular plane. For example, the band observed at 732 cm^{-1} is due to all hydrogens of the outer phenyl rings moving in-phase through the molecular plane (equivalent to the strongest IR active ν_{11} mode in neutral benzene at 673 cm^{-1}; Wilson 1934) with the two hydrogens of the middle phenyl ring moving out of phase.

The 2H-loss channel is, as discussed above, a strong, low-energy loss channel. While the IRMPD spectrum obtained by solely integrating the ion current in this channel exhibits strong saturation for the modes clearly visible in the depletion spectrum, it also shows some weaker resonances that are not (clearly) apparent in the depletion spectrum. The IRMPD spectra recorded via the 2H-loss channel are depicted in red. The 500–680 cm^{-1} spectral region is recorded in the same experiment as the depletion spectrum. For the 200–400 cm^{-1} spectral range, the experiment was performed in the FELICE focus, thereby increasing the power density by a factor of 30. When the experiment is performed under the same conditions as

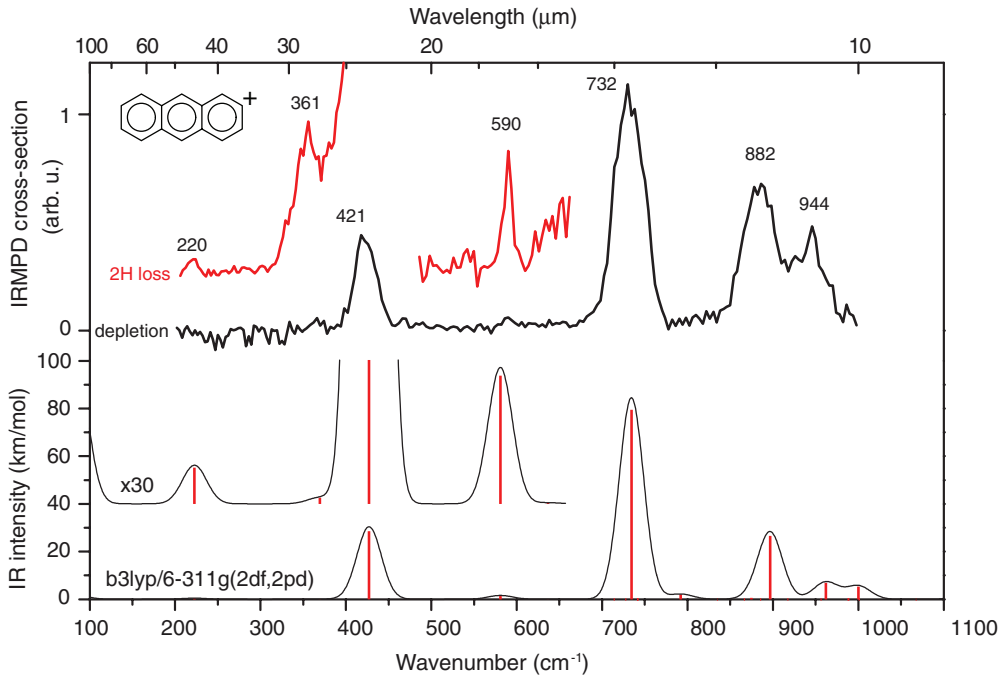

Figure 2. IRMPD spectrum of the anthracene cation via depletion spectroscopy (top, black) and fragmentation into the 2H-loss channel (top, red); the calculated linear absorption spectrum at the B3LYP/6-311g(2df,2pd) level and a convolution with a Gaussian lineshape (15 cm^{-1} Gaussian width). The inset is a vertical zoom by a factor of 30 of the calculated spectra.

(A color version of this figure is available in the online journal.)

Table 1
Observed IRMPD Resonances for the Anthracene Cation

Observed (cm^{-1})	Calculated (cm^{-1})	MI (cm^{-1})	IR Intensity (km mol^{-1})	Mode Description
220	220		0.42	i.p. skeletal deformation
361	365		0.07	o.o.p. skeletal deformation
421	422	432	28.59	In-phase C–H o.o.p. bend
590	574		1.49	i.p. skeletal deformation
732	726	748	79.46	Out-of-phase C–H o.o.p. bend, outer phenyls
882	887	912	26.52	Out-of-phase C–H o.o.p. bend
944	951		6.83	Out-of-phase C–H o.o.p. bend

Note. MI data taken from Hudgins & Allamandola (1995a) and Szczepanski et al. (1993).

for the depletion spectrum, no fragmentation is observed below 421 cm^{-1}.

In the 2H-loss channel three more resonances appear at 220, 361, and 590 cm^{-1}, respectively. While one could argue that the 590 cm^{-1} resonance is visible in the depletion spectrum, this is clearly not the case for the resonances at lower wavenumbers. The comparison between experimental and calculated spectra, which is facilitated by a zoom of the calculated spectrum in Figure 2, also shows an excellent agreement for these weaker resonances. These weaker vibrations are all only weakly IR active skeletal deformations and carry at most a (calculated) integrated IR intensity of 1.5 km mol^{-1}. One notices that the 361 cm^{-1} resonance is substantially stronger than the one at 220 cm^{-1} even though the calculations suggest the opposite (0.42 and 0.07 km mol^{-1} for the bands at 220 and 361 cm^{-1}, respectively). Although the absolute difference in calculated intensity is very small, the reversed relative intensities may also be induced by the multiple photon excitation mechanism; the transition frequency of the strong 421 cm^{-1} mode redshifts once several 361 cm^{-1} photons are absorbed, thereby pushing the 421 cm^{-1} mode into resonance with the laser radiation, facilitating the absorption of further IR photons. Such artificial enhancement of closely spaced bands is a common feature in IRMPD experiments (Oomens et al. 2006).

How do the observed frequencies compare to MI spectra? Szczepanski & Vala (1993) report two resonances below 1000 cm^{-1}: one at 432 cm^{-1} and the other at 912 cm^{-1}. The 432 cm^{-1} feature nicely matches the present 421 cm^{-1} band. Hudgins & Allamandola (1995a) confirm the resonance at 912 cm^{-1} and report an additional resonance at 748 cm^{-1}. Taking into account the IRMPD redshift discussed above, we can assign the 732 and 882 cm^{-1} IRMPD resonances to the 748 and 912 cm^{-1} bands in the MI spectra, respectively. This would constitute a 3% redshift of the IRMPD bands compared to the band positions in the MI spectra. The 944 cm^{-1} IRMPD resonance would then originate from a band around 976 cm^{-1} in the MI spectrum. While a feature may be visible in the spectrum of Szczepanski & Vala (1993) around this frequency, it is so weak that the authors did not consider it a resonance; the same spectral region is not reported on by Hudgins & Allamandola (1995a).

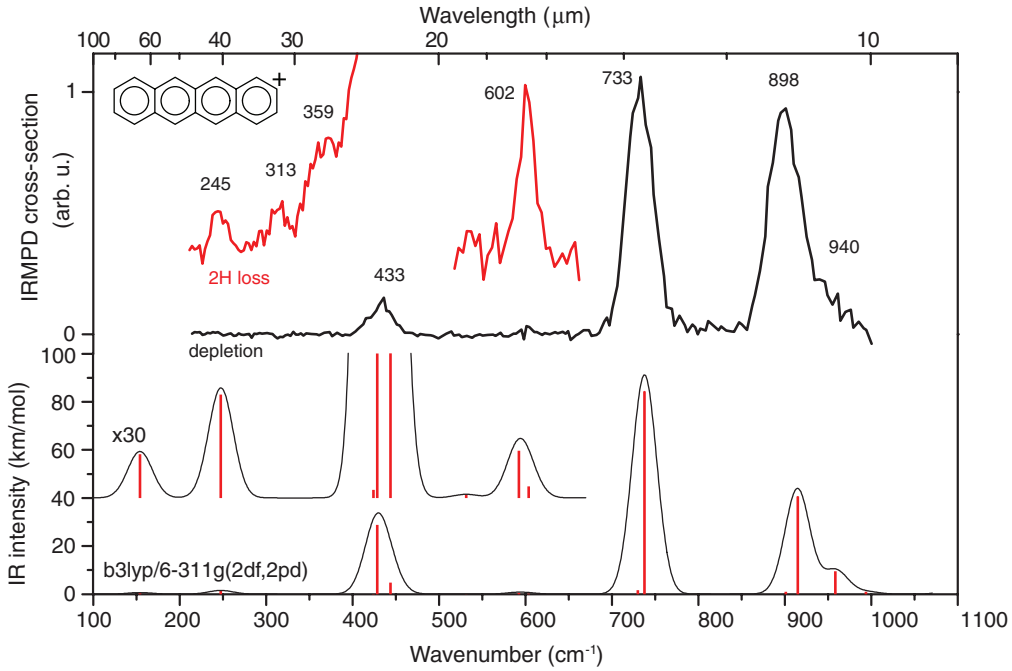

Figure 3. IRMPD spectrum of the tetracene cation via depletion spectroscopy (top, black) and fragmentation into the 2H-loss channel (top, red); the calculated linear absorption spectrum at the B3LYP/6-311g(2df,2pd) level and a convolution with a Gaussian lineshape (15 cm^{-1} Gaussian width). The inset is a vertical zoom by a factor of 30 of the calculated spectra.

(A color version of this figure is available in the online journal.)

Table 2
Observed IRMPD Resonances for the Tetracene Cation

Observed (cm^{-1})	Calculated (cm^{-1})	MI (cm^{-1})	IR intensity (km mol^{-1})	Mode Description
245	245		1.4	o.o.p. skeletal deformation
313				
359				
433	424		28.8	In-phase C–H o.o.p. bend
602	586		0.7	i.p. skeletal deformation
733	730	767	84.3	In-phase C–H o.o.p. bend, outer phenyls
898	905	929	40.7	In-phase C–H o.o.p. bend, inner phenyls
940	949		9.5	Out-of-phase C–H o.o.p. bend

Note. MI data taken from Hudgins & Allamandola (1995a) and Szczepanski et al. (1995a).

3.2. Tetracene

In Figure 3, the IRMPD depletion spectrum for tetracene is displayed; the frequencies of all observed resonances are included in Table 2. A shoulder on the blue side of the 898 cm^{-1} resonance is interpreted as a separate resonance. Its line position at 940 cm^{-1} is determined by fitting the experimental data with two Gaussian functions. There is a reasonable agreement between calculated and observed spectra, especially for the four resonances seen in depletion. They correspond to CH o.o.p. bending vibrations. The relative intensities for the three main resonances appear not that well reproduced by theory. It is known that the IRMPD process can induce deviations in relative intensities as compared to linear absorption (Oomens et al. 2003).

The spectrum recorded in the 2H-loss channel is displayed in red. Here, additional resonances at 245, 313, 359, and 602 cm^{-1} are observed. As for anthracene, the 200–400 cm^{-1} spectral range is recorded in the FELICE focus, as otherwise no dissociation is observed. The resonances at 245 and 602 cm^{-1} are well reproduced by the calculations, assigning these modes as skeletal vibrations. However, the distinct resonances at 313 and 359 cm^{-1} are not accounted for by theory. A possible explanation is that these are due to combination modes. Assuming that at least one of the contributing fundamental modes is IR active, a combination of the IR active 245 cm^{-1} mode and the low-frequency 85 cm^{-1} mode is a candidate for the 313 cm^{-1} resonance. Combination of the fundamental modes at 245 and 136 cm^{-1} could similarly explain the 359 cm^{-1} band in the IRMPD spectrum. Both bands observed are redshifted compared to the computed combination frequency by a factor of about 0.94, which could be accounted for by the cross-anharmonicity between the fundamentals making up the combination mode. The question may arise why combination modes would be visible in this spectral range and not at shorter wavelengths. It must be pointed out that this wavelength range is the only range measured at the highest IR fluences available in the focus, as only then do IR resonances become observable. If the shorter wavelength spectral range is measured at similar IR fluences (not shown), an almost continuous (i.e., unresolved) fragmentation signal is observed.

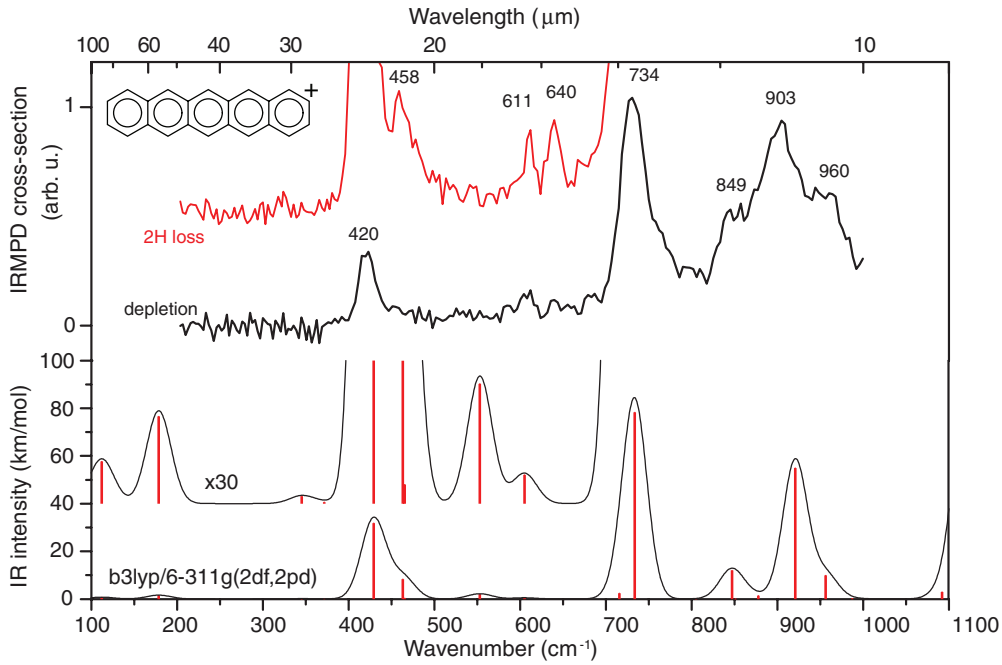

Figure 4. IRMPD spectrum of the pentacene cation via depletion spectroscopy (top, black) and fragmentation into the 2H-loss channel (top, red); the calculated linear absorption spectrum at the B3LYP/6-311g(2df,2pd) level and a convolution with a Gaussian lineshape (15 cm^{-1} Gaussian width). The inset is a vertical zoom by a factor of 30 of the calculated spectra.

(A color version of this figure is available in the online journal.)

Table 3
Observed IRMPD Resonances for the Pentacene Cation

Observed (cm^{-1})	Calculated (cm^{-1})	MI (cm^{-1})	IR Intensity (km mol^{-1})	Mode Description
420	425		31.76	In-phase C–H o.o.p. bend, middle phenyls
458	458		8.38	Out-of-phase C–H o.o.p. bend, middle phenyls
611				
640				
734	726	749	78.26	Out-of-phase C–H o.o.p bend, terminating phenyls
849	838	862	11.98	Out-of-phase C–H o.o.p bend, middle phenyls
903	911	934	54.89	In-phase C–H o.o.p. bend, middle phenyls
960	946		9.89	In-phase C–H o.o.p. bend, outer phenyls

Note. MI data are from Hudgins & Allamandola (1995a) and Szczepanski et al. (1995b).

MI spectra reveal two resonances, at 767 and 929 cm^{-1} (Hudgins & Allamandola 1995a; Szczepanski et al. 1995a), which are probably the equivalents of the 733 and 898 cm^{-1} resonances in the IRMPD spectrum.

3.3. Pentacene

Unlike for the smaller PAH cations, spectrally unresolved depletion signals tend to become apparent even at moderate IR fluences in the IRMPD depletion spectrum for the pentacene radical cation, as is clear from the nonzero background in Figure 4. However, on top of this background three clear resonances can be distinguished at 420, 734, and 903 cm^{-1}, where the 903 cm^{-1} band exhibits pronounced shoulders at 849 and 960 cm^{-1}. There also appears to be a shoulder to the blue of the 420 cm^{-1} resonance as well as some activity slightly above 600 cm^{-1}. This is more clearly observed when monitoring the 2H-loss channel, where extra resonances can be distinguished at 458, 611, and 640 cm^{-1}. As for the other PAH ions, the 2H-loss channel spectrum in the 200–400 cm^{-1} range is recorded in the FELICE focus. The frequencies of all observed resonances are included in Table 3.

Upon inspection of the calculated spectrum it is evident that the five strong bands observed in the depletion spectrum are well reproduced by the theoretical spectrum. These bands are due to the CH o.o.p. bending vibrations. For the weaker bands the mode assignment is not so straightforward. While the 458 cm^{-1} band matches a calculated CH o.o.p. bending vibration well, there is a clear mismatch between theory and experiment for the 611 and 640 cm^{-1} resonances. At this point, the reason for this mismatch is unclear, and it is rather surprising given the good agreement for anthracene and tetracene using the same density functional theory (DFT) functional and basis set. It is tempting to attribute the 611 and 640 cm^{-1} resonances to the IR active vibrations calculated at 547 and 599 cm^{-1} (both in-plane skeletal deformations), but the discrepancy appears too large to justify this assignment and it should be considered as tentative at most. A calculation of the quartet state, which is computed to lie 1.6 eV higher in energy, does not provide a better spectral match.

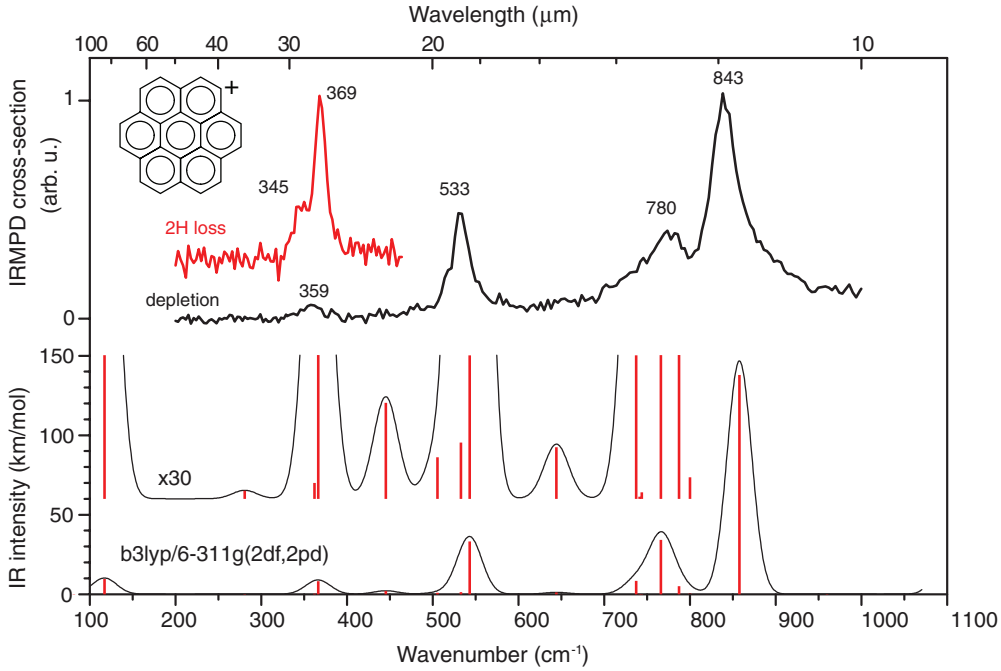

Figure 5. IRMPD spectrum of the coronene cation via depletion spectroscopy (top, black) and fragmentation into the 2H-loss channel (top, red); the calculated linear absorption spectrum at the B3LYP/6-311g(2df,2pd) level and a convolution with a Gaussian lineshape (15 cm^{-1} Gaussian width). The inset is a vertical zoom by a factor of 30 of the calculated spectra.

(A color version of this figure is available in the online journal.)

Table 4
Observed IRMPD Resonances for the Coronene Cation

Observed (cm^{-1})	Calculated (cm^{-1})	MI (cm^{-1})	IR Intensity (km mol^{-1})	Mode Description
345	358		0.33	i.p. skeletal deformation
369	363		8.10	i.p. skeletal deformation
533	538		33.19	(0,1) drumhead mode
780	758		34.08	i.p. skeletal deformation
843	849	875	137.97	In-phase C–H o.o.p. bend

Note. MI data from Hudgins & Allamandola (1995b) and Szczepanski & Vala (1993).

Szczepanski et al. (1995b) report one resonance at 934 cm^{-1}, which corresponds to the 903 cm^{-1} IRMPD band; Hudgins & Allamandola (1995a) report the same value plus one at 862 cm^{-1} (IRMPD: 849 cm^{-1}) and two resonances close to the 734 cm^{-1} IRMPD band, namely a weak band at 740 and a stronger one at 749 cm^{-1}. The band found here at 960 cm^{-1} has no counterpart in the MI spectrum as it falls in a spectral range that is not reported on by Hudgins & Allamandola (1995a). In the spectrum reported by Szczepanski et al. (1995b) the region is shown, but an impurity of the matrix screens possible pentacene cation absorptions near this frequency.

3.4. Coronene

Finally, the IRMPD spectrum for the coronene cation is shown in Figure 5. The depletion spectrum exhibits four distinct resonances at 359, 533, 780, and 843 cm^{-1}, which are all included in Table 4. From a comparison with the calculated spectrum the 780 cm^{-1} and 359 cm^{-1} bands can safely be assigned to in-plane skeletal deformations. There is an overlap between this spectral range and that explored in a previous study from our group (Oomens et al. 2001b). The band previously found at 849 cm^{-1} clearly corresponds to the band at 843 cm^{-1} in the present IRMPD spectrum; the slight discrepancy is likely due to the higher power levels used in the present experiment, leading to a slightly higher anharmonic redshift, and/or to small inaccuracies in the wavelength calibration. It is interesting to see that the 780 cm^{-1} band is relatively much stronger in the present spectrum. This is probably due to the substantial threshold for dissociation of the coronene cation, which is more easily reached with the IR fluences available in FELICE as compared to those in the FELIX experiment of Oomens et al. (2001b). In the MI spectrum the only mode reported is the CH o.o.p. mode at 875 cm^{-1} (Hudgins & Allamandola 1995b) which is the equivalent of the 843 cm^{-1} IRMPD band.

All four major resonances are well matched in the calculated spectrum. Perhaps somewhat led by the calculations, one can even discern weaker bands near 650 and 450 cm^{-1} in the depletion spectrum. The spectrum recorded for the 2H-loss channel (recorded at 110 mm from the FELICE focus) exhibits only a broad, continuous absorption. Interestingly, the 2H-loss channel spectrum reveals that the somewhat broad resonance at 359 cm^{-1} consists of two separate bands at 345 and 369 cm^{-1}. A weakly IR-active in-plane skeletal deformation vibration may be responsible for the 345 cm^{-1} band; its weak IR activity (computed integrated intensity: 0.33 km mol^{-1}) may be overcome by intensity borrowing in the IRMPD excitation mechanism, as described above for the anthracene cation.

4. DISCUSSION AND CONCLUSION

At the IR fluences available in the FELICE experiment, a substantial fragmentation is observed at wavenumbers higher than roughly 400 cm^{-1} (wavelengths shortward of 25 μm). At lower frequencies, fragmentation is observed only in the lowest energy-loss channel and when the highest fluences available are employed. In order to estimate what is the lowest wavenumber

at which IRMPD is feasible in the current experiment, it is necessary to evaluate the IR absorption cross sections as well as the thresholds to unimolecular dissociation.

Ling & Lifshitz (1998) observed $C_{14}H_8^+$ cations after VUV irradiation of a thermal beam of neutral anthracene in approximately the same time window as the current experiment. From these observations we can estimate the number of IR photons that have been absorbed by the anthracene cation at 220 cm^{-1}. If we assume that the internal energy of the anthracene ions produced here is similar to that of the neutrals and that most of the excess energy of the 193 nm photon is carried away by the electron, the difference between the VUV appearance energy of $C_{14}H_8^+$ (∼15 eV) and the ionization potential (7.4 eV) should be made up by IR excitation. This suggests that some 250–300 photons have been absorbed at 220 cm^{-1}. Hence, at the maximum fluence available at 220 cm^{-1}, ∼150 J cm^{-2}, a vibrational mode with a computed IR intensity of 0.4 km mol^{-1} can absorb at least 7 eV of energy.

It is difficult to use this result to predict the minimum integrated absorption intensity of a mode required to permit detection at longer wavelengths, but some general remarks can be made. First, the internal energy to which the ion is excited (which determines the fragmentation rate) is, to a first approximation, assumed to be linearly proportional to the product of photon flux and IR absorption cross section. Of course, the IR absorption cross section is not constant with internal energy and depends on unknown molecular properties such as the anharmonicity of the specific vibrational mode. Also, the rate of excitation is dependent on the rate of intramolecular vibrational energy distribution (Lehmann et al. 1994); if this rate is not sufficiently high, the ion cannot continue to absorb photons in the vibrational mode.

Second, the laser waist is proportional to the square root of the wavelength. For a constant energy per laser pulse this means that the photon flux is wavelength independent. The internal energy to which an ion in the current experimental geometry is excited per unit of IR absorption cross section at a fixed laser pulse energy is thus, to a first approximation, only dependent on the energy carried per photon absorbed, and thus inversely proportional to the wavelength.

However, the fragmentation rate grows exponentially with internal energy and at an unknown internal energy threshold surpasses the 10^5 s^{-1} required for detection in this experiment. There exists thus a regime where the onset of fragmentation occurs rather rapidly, which has been observed experimentally for, e.g., coronene–Fe^+ complexes (Simon et al. 2008). Given the fact that the weakly IR-active vibrational modes at lower wavenumber are only observed in the focus it appears unlikely that resonances with IR absorption intensities below 1 km mol^{-1} can be detected very far beyond 50 μm for systems with a similar dissociation energy as anthracene.

Not surprisingly, the experimental spectra of all cations studied here are predicted rather well at the current level of DFT calculations. Interestingly, the frequencies of some weaker observed bands are not matched well by the calculations. Especially the 611 cm^{-1} and 640 cm^{-1} bands for the pentacene cation exhibit discrepancies with the calculations.

For all calculated spectra we have used the same scaling factor of 0.94. This is a somewhat lower scaling factor than generally employed, even when taking into account that the IRMPD process typically redshifts the observed band with respect to the fundamental frequency (Oomens et al. 2006). It is likely that the rather high fragmentation energies of PAHs require them to be highly excited for fragmentation to occur and that the IRMPD mechanism leads to a rather large redshift which is mirrored in the lower scaling factor.

Nevertheless, an excellent match between calculated and experimental spectra is obtained. It is of interest to note that the scaling factor used is uniform over the entire spectral range studied, which spans a factor of five, and that it is the same for all species. The good agreement with the experiment also suggests that there is no need for different scaling factors for different vibrational modes probed in this spectral range.

It has been pointed out earlier that the CH o.o.p. bending vibrations, for which it is generally accepted that they are responsible for the UIRs between 11 and 15 μm, exhibit characteristic frequencies depending on the number of adjacent CH groups on an aromatic ring (Hudgins & Allamandola 1999). In the present observations, all catacondensed PAH cations exhibit a band within a few wavenumbers of 733 cm^{-1}. The associated vibrations are CH o.o.p. vibrations of the outer phenyl rings of the ion, which possess four adjacent CH units. It is striking that the vibrational frequencies are so close for different sized ions; moreover, the fact that they fall very close to the 13.6 μm UIR feature experimentally confirms the proposed assignment of this feature to so-called quarto CH o.o.p. bending modes (Hudgins & Allamandola 1999).

For the larger species, pentacene and coronene, the baseline does not go to zero at wavenumbers higher than approximately 400 cm^{-1}, i.e., there is always a small amount of depletion. We attribute this to the rapidly increasing number of combination modes with increasing frequency, which cannot be resolved but form a continuous background absorption. The density of combination modes per cm^{-1} increases rapidly with the size of the ion, and the presence of many, albeit weakly IR active, combination modes induces a non-negligible IR absorption. Such a continuum is inherent to larger molecular systems and has also been observed in IR emission experiments (Williams & Leone 1995).

In conclusion, we have presented the first gas-phase spectra of cationic PAHs in the far-IR range down to 200 cm^{-1}, thereby constituting the first IRMPD spectra of strongly bound species down to these frequencies. The spectra exhibit clear and sharp resonances which may assist in the interpretation of interstellar observations in the far-IR spectral domain. In general, a good agreement with theoretical spectra is found. The laboratory observation of bands at 733 cm^{-1} for all linear PAH cations confirms the proposed assignment of the 13.6 μm UIR feature to CH o.o.p. bending modes of peripheral phenyl rings containing four adjacent CH bonds.

This work is part of the research program of FOM, which is financially supported by the Nederlandse Organisatie voor Wetenschappelijk Onderzoek (NWO). The construction of the FELICE beam line was funded by NWO through the NWO-Groot scheme. The authors thank the excellent support by the FELIX staff, in particular J. Pluijgers for his help in constructing the sublimation source. J.O. acknowledges the Stichting Physica.

REFERENCES

Allamandola, L. J., Tielens, A., & Barker, J. R. 1985, ApJ, 290, L25
Andersen, M. P., & Uvdal, P. 2005, J. Phys. Chem. A, 109, 2937
Bakker, J. M., Lapoutre, V. J. F., Redlich, B., et al. 2010, J. Chem. Phys., 132, 074305
Barker, J. R., Allamandola, L. J., & Tielens, A. 1987, ApJ, 315, L61

Bauschlicher, C. W., Jr., Boersma, C., Ricca, A., et al. 2010, ApJS, 189, 341
Boersma, C., Bauschlicher, C. W., Ricca, A., et al. 2011, ApJ, 729, 64
Cami, J., Bernard-Salas, J., Peeters, E., & Malek, S. E. 2010, Science, 329, 1180
Cook, D. J., & Saykally, R. J. 1998, ApJ, 493, 793
De Vries, M. S., Reihs, K., Wendt, H. R., et al. 1993, Geochim. Cosmochim. Acta, 57, 933
Ekern, S. P., Marshall, A. G., Szczepanski, J., & Vala, M. 1998, J. Phys. Chem. A, 102, 3498
Frisch, M. J., Trucks, G. W., Schlegel, H. B., et al. 2004, Gaussian 03 (Wallingford, CT: Gaussian, Inc.)
Houck, J. R., Roellig, T. L., van Cleve, J., et al. 2004, ApJS, 154, 18
Hudgins, D. M., & Allamandola, L. J. 1995a, J. Phys. Chem., 99, 8978
Hudgins, D. M., & Allamandola, L. J. 1995b, J. Phys. Chem., 99, 3033
Hudgins, D. M., & Allamandola, L. J. 1997, J. Phys. Chem. A, 101, 3472
Hudgins, D. M., & Allamandola, L. J. 1999, ApJ, 516, L41
Hudgins, D. M., Bauschlicher, C. W., Allamandola, L. J., & Fetzer, J. C. 2000, J. Phys. Chem. A, 104, 3655
Hudgins, D. M., Sandford, S. A., & Allamandola, L. J. 1994, J. Phys. Chem., 98, 4243
Joblin, C., Boissel, P., Leger, A., Dhendecourt, L., & Defourneau, D. 1995, A&A, 299, 835
Joblin, C., d'Hendecourt, L., Léger, A., & Défourneau, D. 1994, A&A, 281, 923
Jochims, H. W., Baumgärtel, H., & Leach, S. 1999, ApJ, 512, 500
Léger, A., & Puget, J. L. 1984, A&A, 137, L5
Lehmann, K. K., Scoles, G., & Pate, B. H. 1994, Annu. Rev. Phys. Chem., 45, 241
Ling, Y., & Lifshitz, C. 1998, J. Phys. Chem. A, 102, 708
Ling, Y., Martin, J. M. L., & Lifshitz, C. 1997, J. Phys. Chem. A, 101, 219
Mattioda, A. L., Hudgins, D. M., Bauschlicher, C. W., Rosi, M., & Allamandola, L. J. 2003, J. Phys. Chem. A, 107, 1486
Mattioda, A. L., Ricca, A., Tucker, J., Bauschlicher, C. W., & Allamandola, L. J. 2009, AJ, 137, 4054
Okumura, M., Yeh, L. I., & Lee, Y. T. 1985, J. Chem. Phys., 83, 3705
Oomens, J., Meijer, G., & von Helden, G. 2001a, J. Phys. Chem. A, 105, 8302
Oomens, J., Sartakov, B. G., Meijer, G., & von Helden, G. 2006, Int. J. Mass Spectrom., 254, 1
Oomens, J., Sartakov, B. G., Tielens, A., Meijer, G., & von Helden, G. 2001b, ApJ, 560, L99
Oomens, J., Tielens, A., Sartakov, B. G., von Helden, G., & Meijer, G. 2003, ApJ, 591, 968
Oomens, J., van Roij, A. J. A., Meijer, G., & von Helden, G. 2000, ApJ, 542, 404
Piest, H., von Helden, G., & Meijer, G. 1999, ApJ, 520, L75
Piest, J. A., Oomens, J., Bakker, J., von Helden, G., & Meijer, G. 2001, Spectrochim. Acta A, 57, 717
Pilbratt, G. L., Riedinger, J. R., Passvogel, T., et al. 2010, A&A, 518, L1
Ricca, A., Bauschlicher, C. W., Mattioda, A. L., Boersma, C., & Allamandola, L. J. 2010, ApJ, 709, 42
Ricks, A. M., Douberly, G. E., & Duncan, M. A. 2009, ApJ, 702, 301
Sellgren, K., Werner, M. W., Ingalls, J. G., et al. 2010, ApJ, 722, L54
Simon, A., Joblin, C., Polfer, N., & Oomens, J. 2008, Phys. Chem. A, 112, 8551
Szczepanski, J., Drawdy, J., Wehlburg, C., & Vala, M. 1995a, Chem. Phys. Lett., 245, 539
Szczepanski, J., & Vala, M. 1993, ApJ, 414, 646
Szczepanski, J., Vala, M., Talbi, D., Parisel, O., & Ellinger, Y. 1993, J. Chem. Phys., 98, 4494
Szczepanski, J., Wehlburg, C., & Vala, M. 1995b, Chem. Phys. Lett., 232, 221
Tielens, A. 2008, ARA&A, 46, 289
Wang, X. K., Lin, X. W., Mesleh, M., et al. 1995, J. Mater. Res., 10, 1977
Wang, X. M., Becker, H., Hopkinson, A. C., et al. 1997, Int. J. Mass Spectrom. Ion Process., 161, 69
Werner, M. W. 2004, ApJS, 154, 1
Williams, R. M., & Leone, S. R. 1995, ApJ, 443, 675
Wilson, E. B. 1934, Phys. Rev., 45, 706
Zhang, J., Han, F. Y., Pei, L. S., Kong, W., & Li, A. G. 2010, ApJ, 715, 485
Zhang, J., Pei, L. S., & Kong, W. 2008, J. Chem. Phys., 128, 104301